Research article
DOI: https://doi.org/10.18721/JPM.18415

THE RESPONSE OF AN INTERMODAL FIBER-OPTIC INTERFEROMETER WITH SMSMS STRUCTURE IN CASE OF SPECTRAL INTERROGATION TO CHANGES IN THE REFRACTIVE INDEX OF THE EXTERNAL ENVIRONMENT

L. D. Zavalishina[1], *A. A. Markvart*✉[1], *A. E. Zaripov*[1], *M. A. Bisyarin*[2], *L. B. Liokumovich*[1], *N. A. Ushakov*[1]

[1] Peter the Great St. Petersburg Polytechnic University, St. Petersburg, Russia

[2] St. Petersburg State University, St. Petersburg, Russia

✉ markvart_aa@spbstu.ru

Abstract. The operation of an intermode fiber-optic interferometer with "Singlemode-Multimode-Singlemode-Multimode-Singlemode" (SMSMS) structure during its spectral interrogation in the *C*-wavelength range has been studied. The refractive index *n* of the external environment can be measured using this device by providing the interference between fundamental and cladding modes in this structure. The theoretical expressions for calculating the spectral characteristic (SC) of the interferometer were presented, the structures' modes were obtained, the behavior of the SC interference components related to the pairwise interference between the fundamental and cladding modes of a single-mode fiber when *n* changing was analyzed. The methodological errors of *n* measuring the external environment were estimated. The minimum error in *n* determining was $1.7 \cdot 10^{-4}$ in the *n* range from 1.32 to 1.36, which corresponds to a 0.13% change in the range of glycerol concentration from 0 to 25% in the water solution.

Keywords: intermode fiber optic interferometer, SMSMS, refractive index sensor, discrete Fourier transform

Funding: The reported study was funded by Russian Science Foundation (Grant No. 23-72-10095).

Citation: Zavalishina L. D., Markvart A. A., Zaripov A. E., Liokumovich L. B., Ushakov N. A., The response of an intermodal fiber-optic interferometer with SMSMS structure in case of spectral interrogation to changes in the refractive index of the external environment. St. Petersburg State Polytechnical University Journal. Physics and Mathematics. 18 (4) (2025) 206–220. DOI: https://doi.org/10.18721/JPM.18415

Научная статья
УДК 535.3, 535-15, 535.417
DOI: https://doi.org/10.18721/JPM.18415

ОТКЛИК МЕЖМОДОВОГО ВОЛОКОННО-ОПТИЧЕСКОГО ИНТЕРФЕРОМЕТРА С SMSMS-СТРУКТУРОЙ ПРИ СПЕКТРАЛЬНОМ ОПРОСЕ НА ИЗМЕНЕНИЕ ПОКАЗАТЕЛЯ ПРЕЛОМЛЕНИЯ ВНЕШНЕЙ СРЕДЫ

Л. Д. Завалишина[1], *А. А. Маркварт*✉[1], *А. Э. Зарипов*[1], *М. А. Бисярин*[2], *Л. Б. Лиокумович*[1], *Н. А. Ушаков*[1]

[1] Санкт-Петербургский политехнический университет Петра Великого, Санкт-Петербург, Россия

[2] Санкт-Петербургский государственный университет, Санкт-Петербург, Россия

✉ markvart_aa@spbstu.ru

Аннотация. Исследовано функционирование межмодового волоконно-оптического интерферометра со структурой “Singlemode- Multimode-Singlemode-Multimode-Singlemode» (SMSMS) при его спектральном опросе в *C*-диапазоне длин волн. Таким интерферометром можно измерять показатель преломления *n* внешней среды путем создания интерференции между фундаментальной и оболочечными модами в этой структуре. Представлены теоретические выражения для расчета спектральной характеристики (СХ) интерферометра, рассчитаны моды этой структуры, проанализировано поведение интерференционных компонент СХ, относящихся к попарной интерференции фундаментальной и оболочечных мод одномодового волокна при изменении *n*. Проведена оценка методических погрешностей измерения *n* внешней среды, которая состояла из раствора глицерина в дистиллированной воде. Минимальная ошибка определения *n* составила $1{,}7 \cdot 10^{-4}$ в диапазоне $n = 1{,}32 - 1{,}36$, что соответствует изменению концентрации глицерина в воде на 0,13% в диапазоне от 0 до 25 %.

Ключевые слова: межмодовый волоконный интерферометр, SMSMS, датчик показателя преломления, дискретное преобразование Фурье

Финансирование: Исследование выполнено за счет гранта Российского научного фонда № 10095-72-23

Ссылка для цитирования: Завалишина Л. Д., Маркварт А. А., Зарипов А. Э., Лиокумович Л. Б., Ушаков Н. А. Отклик межмодового волоконно-оптического интерферометра с SMSMS- структурой при спектральном опросе на изменение показателя преломления внешней среды // Научно-технические ведомости СПбГПУ. Физико-математические науки. 2025. Т. 18. № 4. С. 206–220. DOI: https://doi.org/10.18721/JPM.18415

Introduction

Measuring the refractive index of the surrounding environment is a major problem with wide applications in various fields of industry, science and other spheres of human activity, including the oil and gas industry, construction industry, optical instrumentation, medicine, and much more.

Fiber-optic refractive index sensors are the most attractive type of sensor due to their high accuracy, compact size, durability, flexibility, biocompatibility, intrinsic safety, as well as resistance to electromagnetic interference, chemical corrosion and radiation. Such refractive index sensors can be based on different principles. A direct method for determining the refractive index at a given wavelength involves measuring the reflection coefficient at the interface between the fiber optic probe and the test liquid [1, 2].

However, in some applied problems, it is not necessary to determine the refractive index of a liquid itself, but only to measure the concentration of a certain substance (analyte) in a solution or its variation. Spectral interrogation methods for fiber-optic sensors based on surface plasmon resonance [3–5], Fabry–Perot interferometer [6], intermodal interferometers with single-mode fiber [7–19] are often used in this case. These methods consist in measuring the reflection or transmission spectra of fiber-optic sensors, i.e., the wavelength dependences of reflectance of optical radiation from the sensor or its transmittance through the sensor. For convenience, we refer to this dependence as the spectral characteristic (SC) of the sensor.

A change in the analyte concentration alters the dispersion dependence of the solution's refractive index, leading to a change in the sensor's SC. In particular, the resonance wavelength shifts in the case of a surface plasmon resonance sensor. It is the phase differences between the interfering waves that change in the cases of Fabry–Perot and intermodal interferometer sensors, with consequent changes in the frequencies and initial phases of the quasi-harmonic components of SC. Notably, these devices are called refractive index sensors, even though they should be calibrated for specific analytes in solution. The measurement resolution for analyte concentration in the solution is typically expressed in terms of the minimum detectable change in the refractive index of the solution at one of the wavelengths within the operational range. Typical values of the change in the refractive index for fiber-optic sensors range from 10^{-4} to 10^{-9} RIU (Refractive Index Unit).

While a refractive index sensor based on an intermodal interferometer with single-mode fiber (SMF) is the easiest type to manufacture, it remains the least studied. These interferometers are manufactured by splicing input SMF with one or more sections comprising different types of fibers and/or fibers with different geometric configurations [7–19]. Examples of such fiber-optic structures are the SNS structure (Singlemode–No core–Single mode) [9–11], the SMSMS structure (Singlemode–Multimode–Singlemode–Multimode–Singlemode) [12-15], the structure consisting of an input SMF, a spliced single-mode section with an offset and a second input SMF [16, 17], etc. Such structures have two input SMF and their SC is measured in transmission. Due to mirror symmetry, it is possible to produce structures with similar properties with a reflector, one input SMF, and SC measurements in reflection mode [17, 18]. The length of the sensing section is reduced by half.

The underlying principle behind the measurements of parameters of the surrounding environment by the above-mentioned interferometers is that the phase accumulation of the modes excited in the sensing section of the interferometer depends on the refractive index of the surrounding environment. These are the modes of coreless fiber of the SNS structure, and the cladding modes (excited by short multimode fiber sections several tens of micrometers in length) of standard single-mode fiber in the central section of the SMSMS structure. In this case, the typical length of the sensing section ranges from several to tens of centimeters. Thus, the resulting interference signal depends on the refractive index of the surrounding environment.

Even though numerous studies considered using such interferometers for measuring the parameters of the surrounding environment, most of them were experimental in nature. In addition to the experiment, some papers provide numerical calculations of light propagation in interferometers, carried out in such software as the BeamPROP using the Beam Propagation Method [18, 19] and Comsol Wave Optics Toolbox using the Beam Envelope method [11]. However, such calculations do not allow to identify the causes of the observed SCs of interferometers or find approaches to improving the sensitivity of interferometers to changes in the parameters of the surrounding environment.

To perform such analysis, it is necessary to calculate all the modes (or the most significant ones) propagating in each section of the interferometer, which is a rather cumbersome due to a large number of such modes. For example, there are 46 guided cladding modes at a wavelength of 1.55 μm in standard SMF-28 fiber under axisymmetric excitation. Moreover, the SCs of interferometers are processed by tracking the positions of extrema along the wavelength scale in most of the studies we are aware of. In the general case, their behavior upon changes in the parameters of the surrounding environment may turn out to be largely nonlinear. The reason is that the SC consists of a set of sinusoids, whose number equals the number of pairwise mode combinations. For example, there are as many as 1081 such combinations in the SMF-28 fiber at a wavelength of 1.55 μm, strongly overlapping each other in terms of oscillation frequency. Moreover, since

different modes exhibit differing sensitivities to changes in the refractive index, the frequencies and initial phases of these sinusoids are altered in different ways.

Thus, the resulting SC is generally very complex and difficult to predict. This makes the development of such a sensor an extremely intricate challenge, even with the more advanced signal processing algorithms.

This paper carries out such calculations of the interferometer, analyzing the effectiveness of numerical processing of its spectral characteristics. As an example, we considered an intermodal fiber interferometer with SMF based on a reflective SMSMS structure.

The first section of the article includes two subsections, describing the interferometer's circuit and presenting theoretical expressions for calculating its spectral characteristics under variable analyte concentration in solution. The second section concentrates on the application of the discrete Fourier transform to processing the interferometer SC. The third section contains the final calculations of the interferometer.

Spectral characteristic of intermodal fiber-optic interferometer based on the reflective SMSMS structure

Interferometer circuit. The intermodal fiber-optic interferometer considered in this paper based on the above-mentioned reflective structure consists of an input single-mode fiber (I-SMF), a section several tens of micrometers long made of multimode fiber (MMF) with a larger core diameter than that of the single-mode fiber, a section several tens of centimeters long, sensitive to changes in the refractive index of the surrounding environment (Sen-SM-Sec), and a mirror at the end face of this section (Fig. 1).

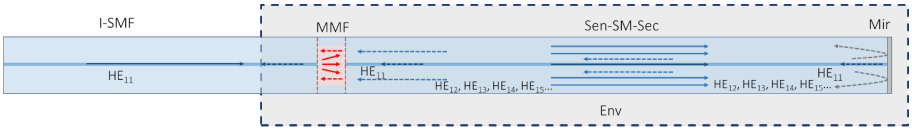

Fig. 1. Circuit of reflective SMSMS structure: input single-mode fiber I-SMF; multimode fiber section MMF; sensing single-mode section Sen-SM-Sec; mirror Mir; surrounding environment Env; modes HE_{ij}; arrows indicate the directions of mode propagation

The HE_{11} mode of I-SMF excites several modes of short MMF, in turn allowing to achieve divergence of the light beam, which is necessary to excite the cladding modes in Sen-SM-Sec. They propagate to the mirror (Mir) at the end of the fiber and return back to MMF, where, again, several modes are excited, generating a complex electric field distribution in the cross-section of I-SMF end face, which is the result of superposition of the fields of the arriving modes. The intensity of the fundamental HE_{11} mode of I-SMF excited by this distribution depends on the phase difference of the modes propagating in the interferometer and should change with a change in the refractive index n of the surrounding environment (Env).

The measured wavelength dependence of the intensity of light reflected from the interferometer, normalized by the intensity of the input radiation, is the spectral characteristic of the interferometer, or, in this case, the actual wavelength dependence of its reflection coefficient.

Calculated theoretical expressions. To calculate the SC of the interferometer, we used a matrix approach taking into account the multimode nature of light propagation in both sections of the interferometer.

The reflection coefficient of the interferometer is equal to the squared modulus that is the product of sequential multiplication of several matrices. The product includes the following:

matrices composed of the mode excitation coefficients at the input to each section;

matrix reflecting the propagation of modes along the MMF section and containing the propagation constants of these modes;

matrix reflecting the propagation of fundamental and cladding modes along Sen-SM-Sec and containing the propagation constants of these modes, as well as a phase shift by π upon reflection from a mirror.

In this case, the expression for the reflection coefficient of the interferometer takes the following form:

$$R = \left| A_{11,1q}^{\mathrm{SM,MM}} e^{-j\beta_{1q}^{\mathrm{MM}} L_{\mathrm{MM}}} A_{1q,1p}^{\mathrm{MM,SM}} e^{-2j\beta_{1p}^{\mathrm{SM}} L_{\mathrm{Sen}} - j\pi} A_{1p,1q}^{\mathrm{SM,MM}} e^{-j\beta_{1q}^{\mathrm{MM}} L_{\mathrm{MM}}} A_{1q,11}^{\mathrm{MM,SM}} \right|^2, \quad (1)$$

where q is the radial number of the axisymmetric HE_{1q} mode in MMF (see Fig. 1); p is the radial number of the axisymmetric HE_{1q} mode in I-SMF ($p = 1$ for the fundamental mode, $p > 1$ for HE_{1p} cladding modes); λ is the light wavelength; L_{MM}, L_{Sen} are the lengths of MMF and Sen-SM-Sec, respectively; β_{1q}^{MM}, β_{1p}^{SM} are the matrices for the propagation constants of HE_{1q} modes in MMF and HE_{1p} modes in Sen-SM-Sec, respectively; $A_{11,1q}^{\mathrm{SM,MM}}$ is the matrix of excitation coefficients of HE_{1q}MM modes in MMF by the fundamental HE_{11} mode of I-SMF; $A_{1q,1p}^{\mathrm{MM,SM}}$ is the matrix of excitation coefficients of the fundamental HE_{11} mode and HE_{1p} cladding modes in Sen-SM-Sec by HE_{1q} modes in MMF; $A_{1q,11}^{\mathrm{SM,MM}}$ is the matrix of excitation coefficients of HE_{1q} modes in MMF by the fundamental HE_{11} mode and HE_{1p} cladding modes in Sen-SM-Sec; $A_{1p,1q}^{\mathrm{MM,SM}}$ is the matrix of excitation coefficients of the fundamental HE_{11} mode by HE_{1q} modes in MMF.

The matrices of mode propagation constants in MMF and Sen-SM-Sec denoted as MM and SM have a diagonal form:

$$\beta_{1q}^{\mathrm{MM}} = \begin{pmatrix} \beta_{11}^{\mathrm{MM}} \ldots 0 \\ 0 \ddots 0 \\ \vdots \quad \vdots \\ 0 \ldots \beta_{1q}^{\mathrm{MM}} \end{pmatrix}, \ \beta_{1p}^{\mathrm{SM}} = \begin{pmatrix} \beta_{11}^{\mathrm{SM}} \ldots 0 \\ 0 \ddots 0 \\ \vdots \quad \vdots \\ 0 \ldots \beta_{1p}^{\mathrm{SM}} \end{pmatrix}. \quad (2)$$

The excitation coefficients of the modes are found by calculating the overlap integral via the following formula:

$$a_{1p,1q}^{\mathrm{SM,MM}} = \frac{\left| \int \mathbf{E}_{1p}^{\mathrm{SM}*} \cdot \mathbf{E}_{1q}^{\mathrm{MM}} dS \right|}{\sqrt{\int \left| \mathbf{E}_{1p}^{\mathrm{SM}} \right|^2 \cdot dS \int \left| \mathbf{E}_{1q}^{\mathrm{MM}} \right|^2 \cdot dS}}, \quad (3)$$

where $\mathbf{E}_{1p}^{\mathrm{SM}}$, $\mathbf{E}_{1q}^{\mathrm{MM}}$ are the vector transverse modal functions (their complex amplitudes) of the exciting HE_{1p} mode of Sen-SM-Sec and the excited mode of MMF (see Fig. 1); dS is the cross-sectional area element of the fiber; the complex conjugation operator is marked with an asterisk.

The matrices of the excitation coefficients are written as follows:

$$A_{1p,1q}^{\mathrm{SM,MM}} = \begin{pmatrix} a_{11,11}^{\mathrm{SM,MM}} a_{11,12}^{\mathrm{SM,MM}} \ldots a_{11,1Q}^{\mathrm{SM,MM}} \\ a_{12,11}^{\mathrm{SM,MM}} \ddots \quad a_{12,1Q}^{\mathrm{SM,MM}} \\ \vdots \quad \vdots \\ a_{1P,11}^{\mathrm{SM,MM}} a_{1P,12}^{\mathrm{SM,MM}} \ldots a_{1P,1Q}^{\mathrm{SM,MM}} \end{pmatrix}, \ A_{1q,1p}^{\mathrm{MM,SM}} = \begin{pmatrix} a_{11,11}^{\mathrm{MM,SM}} a_{11,12}^{\mathrm{MM,SM}} \ldots a_{11,1P}^{\mathrm{MM,SM}} \\ a_{12,11}^{\mathrm{MM,SM}} \ddots \quad a_{12,1Q}^{\mathrm{MM,SM}} \\ \vdots \quad \vdots \\ a_{1Q,11}^{\mathrm{MM,SM}} a_{1P,12}^{\mathrm{MM,SM}} \ldots a_{1Q,1P}^{\mathrm{MM,SM}} \end{pmatrix} = A_{1p,1q}^{\mathrm{SM,MMH}},$$

$$A_{11,1q}^{\mathrm{SM,MM}} = \left(a_{11,11}^{\mathrm{SM,MM}} \ a_{11,12}^{\mathrm{SM,MM}} \ldots a_{11,1Q}^{\mathrm{SM,MM}} \right), A_{1q,11}^{\mathrm{MM,SM}} = \begin{pmatrix} a_{11,11}^{\mathrm{MM,SM}} \\ a_{12,11}^{\mathrm{MM,SM}} \\ \vdots \\ a_{1Q,11}^{\mathrm{MM,SM}} \end{pmatrix} = A_{11,1q}^{\mathrm{SM,MMH}}, \quad (4)$$

where P is the number of considered fundamental and cladding modes in Sen-SM-Sec; Q is the number of considered modes in the MMF; the superscript

H denotes the Hermitian conjugate of the matrix.

Discrete Fourier transform applied to processing of the interferometer's spectral characteristic

It should be noted that MMF has the length of several tens of micrometers (this is four orders of magnitude shorter than the length of Sen-SM-Sec), therefore, the oscillatory component of the interferometer's SC can be approximately written as follows:

$$S(\lambda) \approx \overline{S}(\lambda) + \sum_{\eta=1}^{P} \sum_{\mu=p+1}^{P} s_{1\eta,1\mu}(\lambda) \cdot \cos\left[\Delta\Phi_{1\eta,1\mu}(\lambda)\right], \quad (5)$$

where η, μ are the numbers of the components of axisymmetric interfering modes $HE_{1\eta}$ and $HE_{1\mu}$ of Sen-SM-Sec.

Expression (5) is the sum of the level $\overline{S}(\lambda)$, independent of the phase difference, and cosine components with amplitudes $s_{1\eta,1\mu}(\lambda)$ and arguments expressed as the phase difference of the $HE_{1\eta}$ and $HE_{1\mu}$ modes; this phase difference follows the expression

$$\Delta\Phi^{1\eta,1\mu}(\lambda) = 2L^{\text{Sen}}[\beta^{1\eta}(\lambda) - \beta^{1\mu}(\lambda)],$$

which is in fact equal to the wavenumber $k_0 = 2\pi/\lambda$ multiplied by the OPD of the modes:

$$n_{1\eta}^{eff}(\lambda) \cdot 2L_{Sens} - n_{1\mu}^{eff}(\lambda) \cdot 2L_{Sens}$$

where $n_{1\eta}^{eff}$, $n_{1\mu}^{eff}$ are the effective refractive indices of the modes with the numbers η and μ.

The number of such components is equal to the number of pairwise combinations of HE_{1p} modes equal to $(C_p)^2$.

If the $\Delta\Phi_{1\eta,1\mu}(\lambda)$ dependence is close to linear in the spectral window $\Delta\lambda$ used, while the amplitudes $s_{1\eta,1\mu}$ are nearly wavelength-independent, then the cosine components of the SC can be regarded as harmonic.

Then the cosine argument in Eq. (5) can be described by the following expression:

$$\Delta\Phi_{1\eta,1\mu}(\lambda) \approx \Omega_{1\eta,1\mu} \cdot \lambda + \Theta_{1\eta,1\mu}, \quad (6)$$

and the SC in this spectral window can be regarded as the sum of harmonic components with spatial frequencies $\Omega_{1\eta,1\mu}$ and initial phases $\Theta_{1\eta,1\mu}$. Then the demodulation of the interferometer signal can be reduced to estimation of the frequencies and phases of a polyharmonic SC.

When the interferometer SC is measured, the interrogation system records a sample set S_i, where i is the sample number corresponding to the light wavelength in vacuum, i.e., $S_i = S(\lambda_i)$ in the spectral window $\Delta\lambda$ with the step Δ_λ and the central wavelength λ_0.

Let N be the total number of samples, then the laws of wavelength variation in the second case can be written as

$$\lambda_i = \lambda_0 + [i - (N-1)/2] \cdot \Delta_\lambda,$$

where i varies from 0 to $N-1$, while the scanning range is $\Delta\lambda = \Delta_\lambda \cdot (N-1)$.

In this case, demodulation of the interferometer SC is reduced to estimation of the frequencies and phases of the harmonic components of the following numerical sequence:

$$v(i) = w(i)\left\{\overline{S_i} + \sum_{\eta=1}^{P} \sum_{\mu=p+1}^{P} s_{1\eta,1\mu} \cos\left[\omega_{1\eta,1\mu} \cdot i + \theta_{1\eta,1\mu}\right]\right\}, \quad (7)$$

where $w(i)$ is the weighting window used; $\omega_{1\eta,1\mu}$ are the angular frequencies of the harmonic components of the numerical sequence (measured in rad), $\theta_{1\eta,1\mu}$, rad, are the initial phases.

The angular frequencies are given by the following expressions [20]:

$$\omega_{1\eta,1\mu} = \Delta_\lambda \Omega_{1\eta,1\mu}, \quad (8)$$

$$\theta_{1\eta,1\mu} = \left[\lambda_0 - \Delta\lambda/2\right] \cdot \Omega_{1\eta,1\mu} + \Theta_{1\eta,1\mu}. \quad (9)$$

Frequencies (8) can be found from the peak positions in the Fourier transform modulus of the numerical sequence $v(i)$. The phase increments $\Delta\theta_{1\eta,1\mu}$ can be found by calculating the increments of the Fourier transform's argument precisely at the corresponding peak, or, alternatively, by calculating the Fourier transform $\Delta\psi(\omega_i)$ at fixed frequencies ω_i near the corresponding maxima.

In the case of a symmetric weighting window $w(i)$, the expression for calculating $\Delta\psi(\omega_i)$ is written as follows:

$$\Delta\psi\left(\omega_i\right) = \lambda_0 \cdot \Delta\Omega_{1\eta,1\mu} + \Delta\Theta_{1\eta,1\mu}. \tag{10}$$

The points of the Fourier transform of the numerical sequence can be found directly by calculating the discrete Fourier transform (DFT). To achieve a finer sampling of the Fourier transform, the sequence $v(i)$ can be zero-padded before applying the DFT [20]. Additionally, to reduce errors in estimating frequencies and phases, it is advisable to use custom windows instead of a rectangular window, for example, Hann, Hamming, Blackman, Chebyshev windows, etc. [20].

Thus, a change in the refractive index of the surrounding environment alters the propagation constants of the interfering modes. This in turn leads to a change in the spatial frequencies $\Omega_{1\eta,1\mu}$ and initial phases $\Theta_{1\eta,1\mu}$ of the SC, manifesting as a shift in the positions of the corresponding peaks of the Fourier transform of the detected SC, as well as a change in the arguments of the Fourier transform near these peaks.

Calculations of interferometer and processing of its spectral characteristics via discrete Fourier transform

Numerical simulation was performed for the following characteristics of the interferometer (see Fig. 1):

the range of the light wavelength λ = 1.51–1.59 μm, step $\Delta\lambda$ = 0.16 nm;

model of SMF-28 section included a silica core with a diameter of 8.2 μm (silica was doped with 3.5% germanium) and silica cladding with a diameter of 125 μm;

model of Thorlabs GIF625 MMF included a silica core with a diameter of 62.5 μm (silica was doped with 8.5% germanium in the center of the core cross-section) and a silica shell with a diameter of 125 μm;

length of MMF section L_{MM} = 50 μm;

length of Sen-SM-Sec fiber L_{Sen} = 27 cm;

The surrounding environment consisted of a glycerol solution in distilled water in the mass concentration range of 0–25% at a temperature of 23 °C.

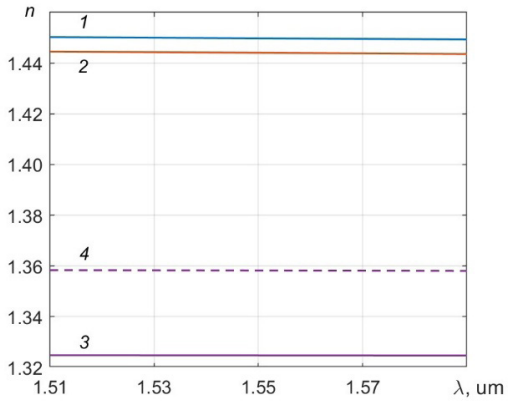

Fig. 2. Dispersion dependences of refractive indices for the media included in SMSMS structure:
fiber core *1*, its cladding *2*, external aqueous environment *3*, 25% aqueous glycerol solution *4* (also a simulated external environment)

Dispersion dependences of the refractive indices of the core, cladding and surrounding environment (i.e., their dependence on the light wavelength) should be obtained for numerical simulations of optical fibers. The approaches proposed in [21–23] were used to calculate the dispersion dependences of silica with germanium oxide dopants at a temperature of 23 °C. Data from [24, 25] were used to calculate the dispersion dependence of water at the same temperature, and data from [26] were used to calculate the dispersion dependence of glycerol. The dispersion dependence of the aqueous glycerol solution was calculated based on the assumption that the refractive index of this solution varies linearly depending on glycerol mass fraction [27]. The corresponding dependences are shown in Fig. 2.

Numerical simulation of the fibers in the interferometer was carried out by numerically solving the wave equation using the finite element method for an electric field in the given

frequency domain. The Helmholtz equation for the electric field was numerically solved at a given frequency, and then a wave solution was sought. The field distributions and effective refractive indices were calculated for the fundamental mode and the first 15 axisymmetric HE_{1p}-type cladding modes of Sen-SM-Sec within the specified wavelength ranges and glycerol concentrations in water, as well as all seven propagating axisymmetric HE_{1q} core modes of MMF.

The electric field distributions of some of them are shown for MMF and Sen-SM-Sec in Fig. 3,*a* and *b*, respectively. Next, the mode excitation coefficients were calculated (Fig. 3,*c*). It was found that 99.9% of mode energy from I-SMF is transferred to core modes of MMF, and 99.8% of this mode energy is further transferred to the fundamental mode and the first 15 axisymmetric cladding modes of Sen-SM-Sec. The obtained result indicates that the selected number of cladding modes in the SMF section is sufficient to describe the behavior of the SMSMS structure considered in the study.

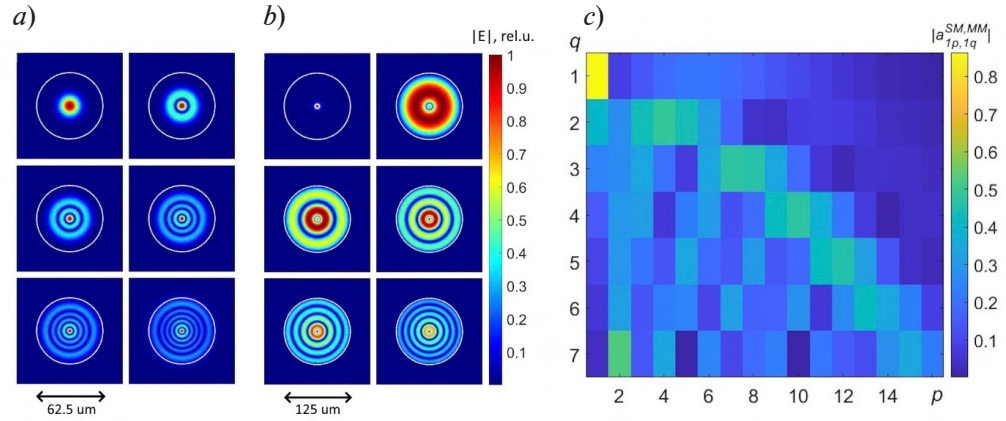

Fig. 3. Calculated electric field strength distributions for first six HE_{1q} modes in MMF (*a*) and Sen-SM-Sec (*b*); coefficients $|a_{1p,1q}^{MM,SM}|$ for exciting HE_{1p} modes in Sen-SM-Sec by HE_{1q} modes of MMF (*c*)

Fig. 4,*a* shows the calculated dependences of the effective refractive index for HE_{1p} modes in Sen-SM-Sec on light wavelength. Figs. 4, *b* and *c* show these dependences for HE_{12} and $HE_{1,16}$ modes, respectively, for pure water and for 25% aqueous glycerol solution. Evidently, as the number of the mode increases, its sensitivity to changes in glycerol concentration increases as well.

As mentioned above, the interference components of the SCs are determined by the cosine arguments $\Delta\Phi_{1\eta,1\mu}(\lambda)$ in expression (5). We established that the components related to interference of the fundamental mode with cladding modes ($\eta = 1$, $\mu = 2-16$) are the most significant in the structure under consideration. Fig. 5 shows these dependences for water and 25% aqueous glycerol solution. Apparently, some of them are rather close to linear, and some are noticeably nonlinear; the result of the latter is that such interference components most likely enter the SC as harmonic, with deeper frequency modulation.

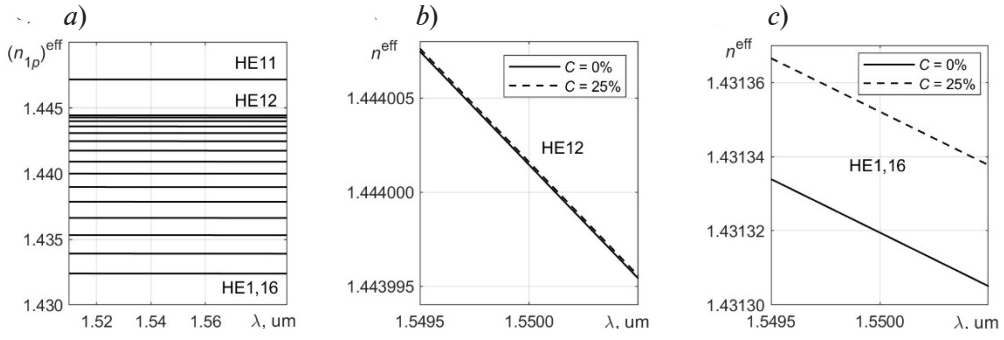

Fig. 4. Dependences of effective refractive index $(n_{1p})^{eff}$ for mode set HE_{1p} in Sen-SM-Sec on light wavelength (*a*); enlarged fragments of these dependences (n^{eff}) for modes HE_{12} (*b*) and $HE_{1,6}$ (*c*), constructed for pure water ($C = 0\%$) and aqueous glycerol solution ($C = 25\%$)

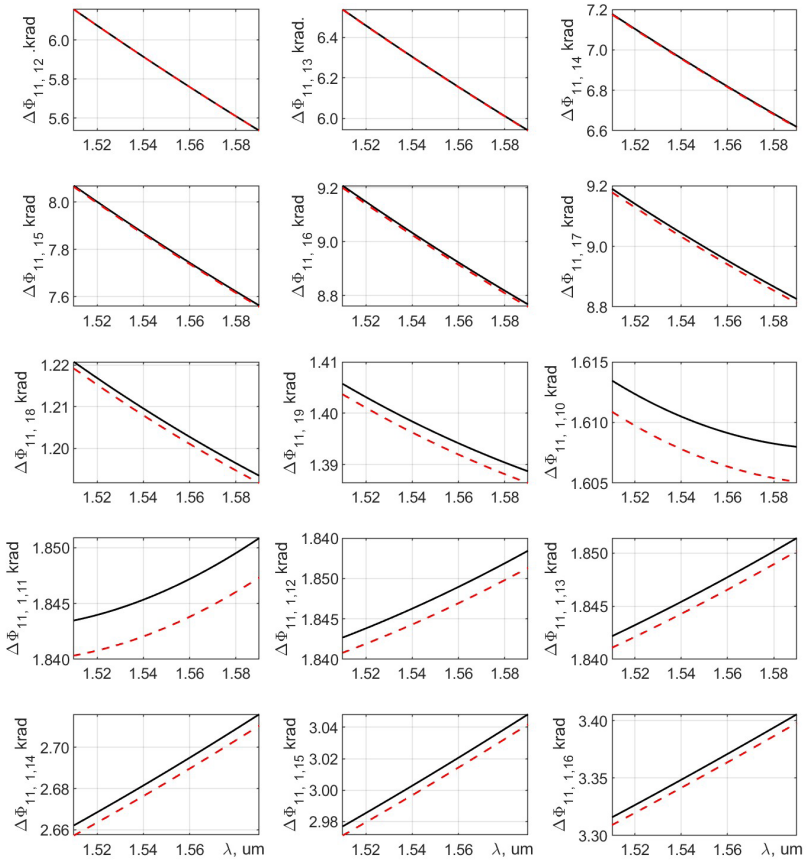

Fig. 5. Dependences of phase difference $\Delta\Phi_{11,1\mu}$ between HE_{11} modes on light wavelength λ for Sen-SM-Sec, constructed for pure water (solid lines) and 25% aqueous glycerol solution (dashed lines)

Next, the quantity $\Delta\Phi_{11,1\mu}(\lambda)$ was fitted to a linear function for each of the components (despite the slight nonlinearity of some of them) for finding the frequencies $\Omega_{11,1\mu}$ and the initial phases $\Theta_{11,1\mu}$ of the corresponding harmonic components. After that, Eqs. (8) and (9) were used to calculate the increments of frequencies ($\Delta\omega_{11,1\mu}$) and phases ($\Delta\theta_{11,1\mu}$) of the harmonic components of the numerical sequence $v(i)$ with a varying concentration of glycerol in water. The calculation results are shown in Fig. 6. As expected, the interference signal of the fundamental and cladding modes turned out to be increasingly sensitive to changes in glycerol concentration with increasing number of the cladding mode.

At the final stage, the spectral characteristics of the interferometer were calculated at various concentrations of glycerol in aqueous solution (Fig. 7). It can be seen that they have a complex oscillating

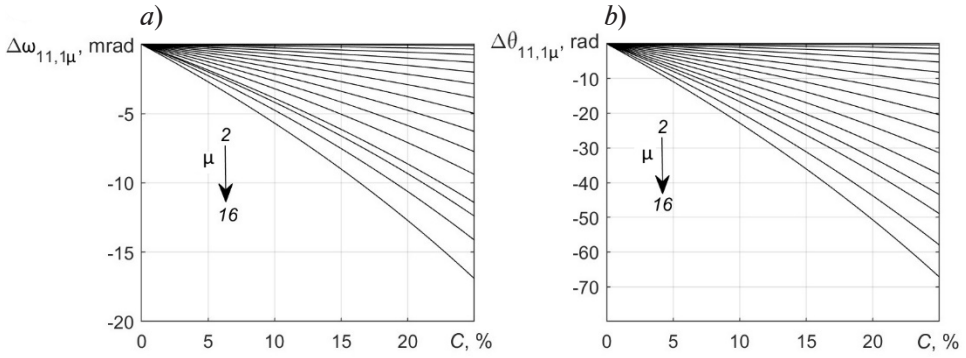

Fig. 6. Increments of frequencies $\Delta\omega_{11,1\mu}$ (*a*) and phases $\Delta\theta_{11,1\mu}$ (*b*) of harmonic components of numerical sequence $v(i)$ as functions of glycerol concentration C in water; arrows indicate the variation in μ

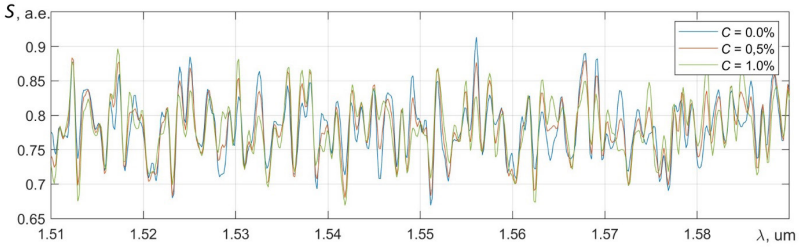

Fig. 7. Calculated spectral characteristics of SMSMS structure for three glycerol concentrations C in aqueous solution

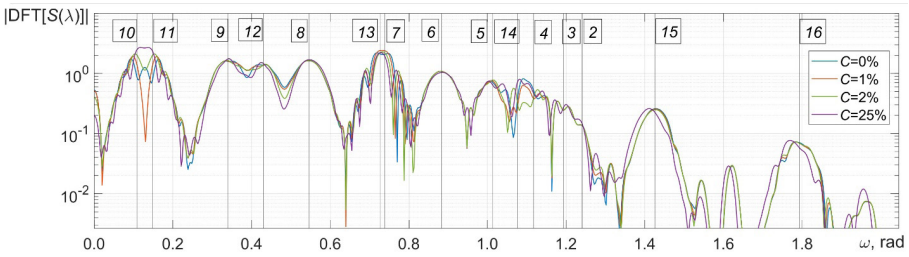

Fig. 8. Calculated Fourier transform moduli for numerical sequences $\nu(i)$ of spectral characteristics of SMSMS structure for four glycerol concentrations C in aqueous solutions
The positions $\omega_{11,1\mu}$ of 15 harmonic interference components corresponding to mode pairs HE_{11}–$HE_{1\mu}$ for μ from *2* to *16* are marked by vertical thin lines with the numbers μ in boxes

character. Fig. 8 shows the Fourier transform moduli of spectral characteristics calculated by DFT, supplemented with SC zeros using the Hann window with the positions of the frequencies $\omega_{11,1\mu}$ indicated for 15 harmonic interference components corresponding to mode pairs HE_{11}–$HE_{1\mu}$ (μ = 16–2). Analyzing the data in Fig. 8, we can conclude that the components with the numbers = ,9 ,8 ,6 ,5 16 ,15 ,12 unambiguously correspond to the Fourier transform peaks. It is worth noting that the peaks are noticeably broadened because the $\Delta\Phi_{11,1\mu}(\lambda)$ dependences deviate from linearity, which can be interpreted as the presence of frequency modulation of harmonic components. The positions of component pairs μ = 2 and μ = 3, μ = 4 and μ = 14, μ = 7 and μ = 13, μ = 10 and μ = 11 are located very close to each other, and, as can be seen from the figure, their responses in the Fourier transform overlap and interfere. The distortion of the shape of the peaks is also caused by the effect of spectral leakage in the DFT (mutual influence of the side lobes of the components). Additionally, while all of these components are influenced by components from mode pairs $HE_{1\eta}$–$HE_{1\mu}$ with numbers $\eta \neq 1$, we find that their amplitude is an order of magnitude smaller, so their influence is less significant. All these undesirable effects introduce systematic errors in estimating the initial phase increments of the harmonic components in the sequence $\nu(i)$ of the SC, which are discussed next.

Fig. 9 shows the calculated results for the increments of the DFT arguments $\Delta\psi(\omega_i)$ from the calculated SCs for the concentration of glycerol in aqueous solution varying from 0 to 25%. The calculated expected values of $\Delta\psi(\omega_i)$ are also given (see Eq. (10)) for complete absence of any sources of systematic error. There are noticeable oscillatory systematic errors for components with numbers μ = 2 – 5, 7, 10, 14, 16, typical for applying DFT to estimating the initial phases of the components of polyharmonic signal.

It should be noted that the mirror counterparts of the components with μ = 1–10 at frequencies $\omega_{11,1\mu} < 0$ were selected in the case of processing by DFT (also at $\omega_{11,1\mu} < 0$), therefore, their corresponding increments $\Delta\psi(\omega_i) > 0$ (in contrast to the phase increments $\Delta\theta_{11,1\mu}$ shown in Fig. 6).

The table gives the final calculation results for the components under consideration: sensitivities of the Fourier transform arguments $\Delta\psi/\Delta C$, rad/%, to the concentration, sensitivities of the Fourier transform arguments $\Delta\psi/\Delta n$, rad/RIU, to the refractive index of the solution at a wavelength of 1.55 μm, systematic errors in determining the glycerol concentration in solution ΔC, %, and refractive index Δn. The smallest errors in determining the glycerol concentration and refractive index were approximately 0.13% and $1.7 \cdot 10^{-4}$ RIU, respectively (highlighted in bold).

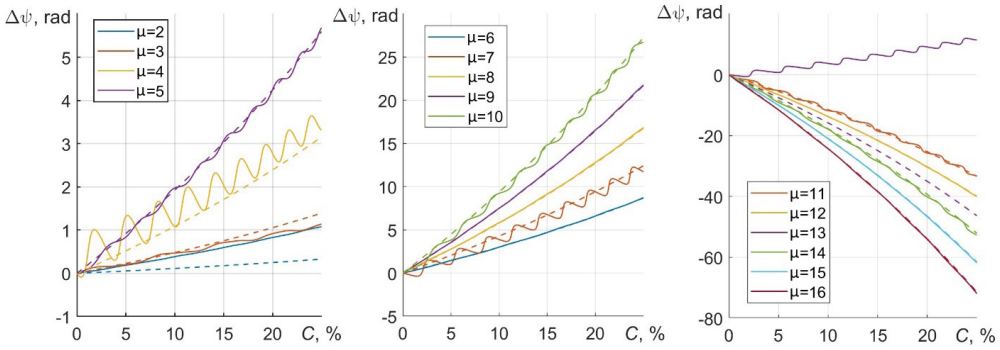

Fig. 9. Increment of DFT arguments $\Delta\psi(\omega_i)$ as function of concentration, obtained by two approaches: from calculated spectral characteristics for the components HE_{11}–$HE_{1\mu}$ (solid lines) and by Eq. (10) (dashed lines) (C is the glycerol concentration in aqueous solution) For clarity, three graphs are given for three groups of values of the number μ

Table

Calculated results for sensitivity parameters of the interferometer's Fourier transform

μ	$\Delta\psi/\Delta C$, rad/%	$\Delta\psi/\Delta n$, rad/RIU	ΔC, %	Δn, 10^{-3} RIU
2	0.013	9.8	57.0	76.0
3	0.056	41.6	4.80	6.40
4	0.130	94.4	6.60	8.80
5	0.220	167	0.67	0.90
6	0.350	260	0.13	0.18
7	0.500	371	2.13	2.85
8	0.670	501	0.16	0.22
9	0.870	650	0.14	0.19
10	1.100	816	0.69	0.92
11	–1.330	–998	0.57	0.76
12	–1.600	–1184	**0.13**	**0.17**
13	–1.850	–1386	31.0	42.0
14	–2.080	–1557	0.60	0.80
15	–2.460	–1840	0.13	0.18
16	–2.860	–2137	0.18	0.24

Notations: μ is the number of the interference component; $\Delta\psi/\Delta C$, $\Delta\psi/\Delta n$ are the sensitivities of the Fourier transform argument to glycerol concentration in aqueous solution and to refractive index at a wavelength of 1.55 μm; ΔC, Δn are the systematic errors in determining the glycerol concentration and the refractive index of optical fiber.

REFERENCES

1. **Xu W., Huang X. G., Pan J. S.,** Simple fiber-optic refractive index sensor based on Fresnel reflection and optical switch, IEEE Sens. J. 13 (5) (2012) 1571–1574.

2. **Brientin A., Leduc D., Gaillard V., et al.,** Numerical and experimental study of a multimode optical fiber sensor based on Fresnel reflection at the fiber tip for refractive index measurement, Opt. Laser Technol. 143 (Nov) (2021) 107315.

3. **Gushchin M. G., Gagarinova D. O., Plyastsov S. A., Vartanyan T. A.,** Development and determination of sensitivity of a fiber-optic refractometer based on surface plasmon resonance, Optics and Spectroscopy. 129 (9) (2021) 1212–1216 (in Russian).

4. **Kazanskiy N. L., Butt M. A., Degtyarev S. A., Khonina S. N.,** Achievements in the development of plasmonic waveguide sensors for measuring the refractive index, Computer Optics. 44 (3) (2020) 295–318 (in Russian).

5. **Mamichev D. A., Kuznetsov I. A., Maslova N. E., Zanaveskin M. L.,** Optical sensors based on surface plasmon resonance for high-sensitive biochemical analysis, Molecular Medicine. (6) (2012) 19–27 (in Russian).

6. **Pevec S., Donlagic D.,** Miniature fiber-optic Fabry-Perot refractive index sensor for gas sensing with a resolution of 5×10^{-9} RIU, Opt. Express. 26 (18) (2018) 23868–23882.

7. **Wang K., Dong X., Kцhler M. H., et al.,** Advances in optical fiber sensors based on multimode interference (MMI): A review, IEEE Sens. J. 21 (1) (2020) 132–142.

8. **Chapalo I., Stylianou A., Mйgret P., Theodosiou A.,** Advances in optical fiber speckle sensing: A comprehensive review, Photonics. 11 (4) (2024) 299.

9. **Mar-Abundis N., Fuentes-Rubio Y. A., Domнnguez-Cruz R. F., Guzmán-Sepúlveda J. R.,** Sugar detection in aqueous solution using an SMS fiber device, Sensors. 23 (14) (2023) 6289.

10. **Li Y., Liu Z., Jian S.,** Multimode interference refractive index sensor based on coreless fiber, Photon. Sens. 4 (March) (2014) 21–27.

11. **Khanikar T., Karki D., Su Y. D., et al.,** Multimode interference-based fiber optic sensors using single mode/no-core/single mode (SNS) configuration, Proc. SPIE. Vol. 13044: Optical Waveguide and Laser Sensors III; Lieberman R. A., Sanders G. A., Buric M. P. (Eds.). 27 June. (2024) 114–122.

12. **Ma Y., Qiao X., Guo T., et al.,** Mach – Zehnder interferometer based on a sandwich fiber structure for refractive index measurement, IEEE Sens. J. 12 (6) (2012) 2081–2085.

13. **Xiong R., Meng H., Yao Q., et al.,** Simultaneous measurement of refractive index and temperature based on modal interference, IEEE Sens. J. 14 (8) (2014) 2524–2528.

14. **Wo J., Sun Q., Li X., et al.,** A compact all fiber refractive index sensor based on modal interference, Proc. IEEE Sens. (1 Oct) (2012) 1–4.

15. **Yusupova L. I., Ivanov O. V.,** Interferometers based on insertions of thin-core optical fibers SM600 and SM450, J. Radioengineering. 83 (9) (2019) 74–78 (in Russian).

16. **Duan D. W., Rao Y. J., Xu L. C., et al.,** In-fiber Mach–Zehnder interferometer formed by large lateral offset fusion splicing for gases refractive index measurement with high sensitivity, Sens. Actuators B-Chem. 160 (1) (2011) 1198–1202.

17. **Tian Z., Yam S. S., Loock H. P.,** Single-mode fiber refractive index sensor based on core-offset attenuators, IEEE Photon. Technol. Lett. 20 (16) (2008) 1387–1389.

18. **Zhang Y., Zhou A., Qin B., et al.,** Refractive index sensing characteristics of single-mode fiber-based modal interferometers, J. Light. Technol. 32 (9) (2014) 1734–1740.

19. **Wang P., Brambilla G., Ding M., et al.,** Investigation of single-mode–multimode–single-mode and single-mode–tapered-multimode–single-mode fiber structures and their application for refractive index sensing, J. Opt. Soc. Am. B. 28 (5) (2011) 1180–1186.

20. **Oppenheim A. V., Schafer R. W.,** Discrete-time signal processing. Pearson New Int. Ed., Pearson Education Limited, London, 2014.

21. **Tripathi S. M., Kumar A., Varshney R. K., et al.,** Strain and temperature sensing characteristics of single-mode–multimode–single-mode structures, J. Light. Technol. 27 (13) (2009) 2348–2356.

22. **Tripathi S. M., Kumar A., Kumar M., Bock W. J.,** Temperature-insensitive fiber-optic devices using multimode interference effect, Opt. Lett. 37 (22) (2012) 4570–4572.

23. **Markel V. A.,** Introduction to the Maxwell Garnett approximation: Tutorial, J. Opt. Soc. Am. A. 33 (7) (2016) 1244–1256.

24. **Kedenburg S., Vieweg M., Gissibl T., Giessen H.,** Linear refractive index and absorption measurements of nonlinear optical liquids in the visible and near-infrared spectral region, Opt. Mater. Express. 2 (11) (2012) 1588–1611.

25. **Abbate G., Bernini U., Ragozzino E., Somma F.,** The temperature dependence of the refractive index of water, J. Phys. D. Appl. Phys. 11 (8) (1978) 1167.

26. **Nyakuchena M., Juntunen C., Shea P., Sung Y.,** Refractive index dispersion measurement in the short-wave infrared range using synthetic phase microscopy, Phys. Chem. Chem. Phys. 25 (34) (2023). 23141–23149.

27. **Takamura K., Fischer H., Morrow N. R.,** Physical properties of aqueous glycerol solutions, J. Pet. Sci. Eng. 98– 99 (Nov) (2012) 50–60.

СПИСОК ЛИТЕРАТУРЫ

1. **Xu W., Huang X. G., Pan J. S.** Simple fiber-optic refractive index sensor based on Fresnel reflection and optical switch // IEEE Sensors Journal. 2012. Vol. 13. No. 5. Pp. 1571–1574.

2. **Brientin A., Leduc D., Gaillard V., Girard M., Lupi C.** Numerical and experimental study of a multimode optical fiber sensor based on Fresnel reflection at the fiber tip for refractive index measurement // Optics & Laser Technology. 2021. Vol. 143. November. P. 107315.

3. **Гущин М. Г., Гагаринова Д. О., Плясцов С. А., Вартанян Т. А.** Создание и определение чувствительности волоконно-оптического рефрактометра на основе поверхностного плазмонного резонанса // Оптика и спектроскопия. 2021. Т. 9 № .129. С. 1216–1212.

4. **Казанский Н. Л., Бутт М. А., Дегтярев С. А., Хонина С. Н.** Достижения в разработке плазмонных волноводных датчиков для измерения показателя преломления // Компьютерная оптика. 2020. Т. 44. № 3. С. 295–318.

5. **Мамичев Д. А., Кузнецов И. А., Маслова Н. Е., Занавескин М. Л.** Оптические сенсоры на основе поверхностного плазмонного резонанса для высокочувствительного биохимического анализа // Молекулярная медицина. 2012. № 6. С. 19–27.

6. **Pevec S., Donlagic D.** Miniature fiber-optic Fabry–Perot refractive index sensor for gas sensing with a resolution of 5×10^{-9} RIU // Optics Express. 2018. Vol. 26. No. 18. Pp. 23868–23882.

7. **Wang K., Dong X., Kцhler M. H., Kienle P., Bian Q., Jakobi M., Koch A. W.** Advances in optical fiber sensors based on multimode interference (MMI): A review // IEEE Sensors Journal. 2020. Vol. 21. No. 1. Pp. 132–142.

8. **Chapalo I., Stylianou A., Мйgret P., Theodosiou A.** Advances in optical fiber speckle sensing: A comprehensive review // Photonics. 2024. Vol. 11. No. 4. P. 299.

9. **Mar-Abundis N., Fuentes-Rubio Y. A., Domнnguez-Cruz R. F., Guzmán-Sepúlveda J. R.** Sugar detection in aqueous solution using an SMS fiber device // Sensors. 2023. Vol. 23. No. 14. P. 6289.

10. **Li Y., Liu Z., Jian S.** Multimode interference refractive index sensor based on coreless fiber // Photonic Sensors. 2014. Vol. 4. March. Pp. 21–27.

11. **Khanikar T., Karki D., Su Y. D., Naeem K., Ohodnicki P.** Multimode interference-based fiber optic sensors using single mode/no-core/single mode (SNS) configuration // Proceedings of SPIE. Vol. 13044: Optical Waveguide and Laser Sensors III. Lieberman R. A., Sanders G. A., Buric M. P. (Eds.). 2024. 27 June. Pp. 114–122.

12. **Ma Y., Qiao X., Guo T., Wang R., Zhang J., Weng Y., Rong Q., Hu M., Feng Zh.** Mach – Zehnder interferometer based on a sandwich fiber structure for refractive index measurement // IEEE Sensors Journal. 2012. Vol. 12. No. 6. Pp. 2081–2085.

13. **Xiong R., Meng H., Yao Q., Huang B., Liu Y., Xue H., Tan Ch., Huang, X.** Simultaneous measurement of refractive index and temperature based on modal interference // IEEE Sensors Journal. 2014. Vol. 14. No. 8. Pp. 2524–2528.

14. **Wo J., Sun Q., Li X., Zhang J., Liu D., Shum P.** A compact all fiber refractive index sensor based on modal interference // Proceedings of IEEE Sensors. 2012. 1 October. Pp. 1–4.

15. **Юсупова Л. И., Иванов О. В.** Интерферометры на основе вставок оптических волокон с тонкой сердцевиной SM600 и SM450 // *Радиотехника*. 2019. Т. 83. № 9. С. 74–78.

16. **Duan D. W., Rao Y. J., Xu L. C., Zhu T., Wu D., Yao J**. In-fiber Mach–Zehnder interferometer formed by large lateral offset fusion splicing for gases refractive index measurement with high sensitivity // Sensors and Actuators B: Chemical. 2011. Vol. 160. No. 1. Pp. 1198–1202.

17. **Tian Z., Yam S. S., Loock H. P.** Single-mode fiber refractive index sensor based on core-offset attenuators // IEEE Photonics Technology Letters. 2008. Vol. 20. No. 16. Pp. 1387–1389.

18. **Zhang Y., Zhou A., Qin B., Deng H., Liu Z., Yang J., Yuan L.** Refractive index sensing characteristics of single-mode fiber-based modal interferometers // Journal of Lightwave Technology. 2014. Vol. 32. No. 9. Pp. 1734–1740.

19. **Wang P., Brambilla G., Ding M., Semenova Y., Wu Q., Farrell G.** Investigation of single-mode–multimode–single-mode and single-mode–tapered-multimode–single-mode fiber structures and their application for refractive index sensing // Journal of the Optical Society of America B. 2011. Vol. 28. No. 5. Pp. 1180–1186.

20. **Oppenheim A. V., Schafer R. W.** Discrete-time signal processing. Pearson New International Edition. London: Pearson Education Limited, 2014. 1047 p.

21. **Tripathi S. M., Kumar A., Varshney R. K., Tripathi S. M., Kumar A., Varshney R. K., Kumar Y. B. P., Marin E., Meunier, J. P.** Strain and temperature sensing characteristics of single-mode–multimode–single-mode structures // Journal of Lightwave Technology. 2009. Vol. 27. No. 13. Pp. 2348–2356.

22. **Tripathi S. M., Kumar A., Kumar M., Bock W. J.** Temperature-insensitive fiber-optic devices using multimode interference effect // Optics Letters. 2012. Vol. 37. No. 22. Pp. 4570–4572.

23. **Markel V. A.** Introduction to the Maxwell Garnett approximation: tutorial // Journal of the Optical Society of America A. 2016. Vol. 33. No. 7. Pp. 1244–1256.

24. **Kedenburg S., Vieweg M., Gissibl T., Giessen H.** Linear refractive index and absorption measurements of nonlinear optical liquids in the visible and near-infrared spectral region // Optical Materials Express. 2012. Vol. 2. No. 11. Pp.1588–1611.

25. **Abbate G., Bernini U., Ragozzino E., Somma F.** The temperature dependence of the refractive index of water // Journal of Physics D: Applied Physics. 1978. Vol. 11. No. 8. P. 1167.

26. **Nyakuchena M., Juntunen C., Shea P., Sung Y.** Refractive index dispersion measurement in the short-wave infrared range using synthetic phase microscopy // Physical Chemistry Chemical Physics. 2023. Vol. 25. No. 34. Pp. 23141–23149.

27. **Takamura K., Fischer H., Morrow N. R.** Physical properties of aqueous glycerol solutions // Journal of Petroleum Science and Engineering. 2012. Vol. 98– 99. November. Pp. 50–60.

THE AUTHORS

ZAVALISHINA Liubov D.
Peter the Great St. Petersburg Polytechnic University
29 Politechnicheskaya St., St. Petersburg, 195251, Russia
l.zavalishina9121@mail.ru
ORCID: 0009-0009-2008-7266

MARKVART Aleksandr A.
Peter the Great St. Petersburg Polytechnic University
29 Politechnicheskaya St., St. Petersburg, 195251, Russia
markvart_aa@spbstu.ru
ORCID: 0000-0001-8080-0830

ZARIPOV Artur E.
Peter the Great St. Petersburg Polytechnic University
29 Politechnicheskaya St., St. Petersburg, 195251, Russia
artur-zaripov-2001@list.ru
ORCID: 0009-0002-1689-6940

BISYARIN Mikhail A.
St. Petersburg State University
7–9 Universitetskaya Emb., St. Petersburg, 199034, Russia
m.bisyarin@spbu.ru
ORCID: 0000-0003-3891-1339

LIOKUMOVICH Leonid L. B.
Peter the Great St. Petersburg Polytechnic University
29 Politechnicheskaya St., St. Petersburg, 195251, Russia
leonid@spbstu.ru
ORCID: 0000-0001-5988-1429

USHAKOV Nikolai A.
Peter the Great St. Petersburg Polytechnic University
29 Politechnicheskaya St., St. Petersburg, 195251, Russia
n.ushakoff@spbstu.ru
ORCID: 0000-0002-3480-2779

СВЕДЕНИЯ ОБ АВТОРАХ

ЗАВАЛИШИНА Любовь Дмитриевна — *стажер-исследователь научной лаборатории волоконной оптики Высшей школы прикладной физики и космических технологий Санкт-Петербургского политехнического университета Петра Великого.*
195251, Россия, г. Санкт-Петербург, Политехническая ул., 29
l.zavalishina9121@mail.ru
ORCID: 0009-0009-2008-7266

МАРКВАРТ Александр Александрович — *кандидат физико-математических наук, доцент Высшей школы прикладной физики и космических технологий Санкт-Петербургского политехнического университета Петра Великого.*
195251, Россия, г. Санкт-Петербург, Политехническая ул., 29
markvart_aa@spbstu.ru
ORCID: 0000-0001-8080-0830

ЗАРИПОВ Артур Эдуардович — *студент Института электроники и телекоммуникаций Санкт-Петербургского политехнического университета Петра Великого.*
195251, Россия, г. Санкт-Петербург, Политехническая ул., 29
artur-zaripov-2001@list.ru
ORCID: 0009-0002-1689-6940

БИСЯРИН Михаил Александрович — *доктор физико-математических наук, ведущий научный сотрудник кафедры радиофизики Санкт-Петербургского государственного университета.*
199034, Россия, г. Санкт-Петербург, Университетская наб., 7–9
bisyarin@spbu.ru
ORCID: 0000-0003-3891-1339

ЛИОКУМОВИЧ Леонид Борисович — *доктор физико-математических наук, профессор Высшей школы прикладной физики и космических технологий Санкт-Петербургского политехнического университета Петра Великого.*
195251, Россия, г. Санкт-Петербург, Политехническая ул., 29
leonid@spbstu.ru
ORCID: 0000-0001-5988-1429

УШАКОВ Николай Александрович — *доктор физико-математических наук, профессор Высшей школы прикладной физики и космических технологий Санкт-Петербургского политехнического университета Петра Великого.*
195251, Россия, г. Санкт-Петербург, Политехническая ул., 29
n.ushakoff@spbstu.ru
ORCID: 0000-0002-3480-2779

Received 07.05.2025. Approved after reviewing 14.05.2025. Accepted 14.05.2025.
Статья поступила в редакцию 07.05.2025. Одобрена после рецензирования 14.05.2025. Принята 14.05.2025.